PROXIMITY TO DEMENTIA ONSET AND MULTI-MODAL NEUROIMAGING CHANGES: THE PREVENT-DEMENTIA STUDY

NeuroImage 229 (2021) 117749

Contents lists available at ScienceDirect

NeuroImage

journal homepage: www.elsevier.com/locate/neuroimage

Proximity to dementia onset and multi-modal neuroimaging changes: The prevent-dementia study

Elijah Mak[a,1,*], Maria-Eleni Dounavi[a,1], Audrey Low[a], Stephen F. Carter[a], Elizabeth McKiernan[a], Guy B Williams[b], P Simon Jones[b], Isabelle Carriere[c], Graciela Terrera Muniz[c], Karen Ritchie[c,d], Craig Ritchie[c], Li Su[a,2], John T O'Brien[a,2]

[a] Department of Psychiatry, School of Clinical Medicine, University of Cambridge, Cambridge Biomedical Campus, Cambridge CB2 0SP, UK
[b] Department of Clinical Neurosciences and Wolfson Brain Imaging Centre, University of Cambridge, Cambridge Biomedical Campus, Cambridge, UK
[c] Centre for Dementia Prevention, University of Edinburgh, Edinburgh, UK
[d] INSERM and University of Montpellier, Montpellier, France

ARTICLE INFO

Keywords:
Dementia
Neuroimaging
Biomarkers
APOE4
MRI
DTI

ABSTRACT

Background: First-degree relatives of people with dementia (FH+) are at increased risk of developing Alzheimer's disease (AD). Here, we investigate "estimated years to onset of dementia" (EYO) as a surrogate marker of pre-clinical disease progression and assess its associations with multi-modal neuroimaging biomarkers.

Methods: 89 FH+ participants in the PREVENT-Dementia study underwent longitudinal MR imaging over 2 years. EYO was calculated as the difference between the parental age of dementia diagnosis and the current age of the participant (mean EYO = 23.9 years). MPRAGE, ASL and DWI data were processed using Freesurfer, FSL-BASIL and DTI-TK. White matter lesion maps were segmented from FLAIR scans. The SPM Sandwich Estimator Toolbox was used to test for the main effects of EYO and interactions between EYO, Time, and APOE-ε4+. Threshold free cluster enhancement and family wise error rate correction ($TFCE_{FWER}$) was performed on voxelwise statistical maps.

Results: There were no significant effects of EYO on regional grey matter atrophy or white matter hyperintensities. However, a shorter EYO was associated with lower white matter Fractional Anisotropy and elevated Mean/Radial Diffusivity, particularly in the corpus callosum ($TFCE_{FWER}$ $p < 0.05$). The influence of EYO on white matter deficits were significantly stronger compared to that of normal ageing. APOE-ε4 carriers exhibited hyperperfusion with nearer proximity to estimated onset in temporo-parietal regions. There were no interactions between EYO and time, suggesting that EYO was not associated with accelerated imaging changes in this sample.

Conclusions: Amongst cognitively normal midlife adults with a family history of dementia, a shorter hypothetical proximity to dementia onset may be associated with incipient brain abnormalities, characterised by white matter disruptions and perfusion abnormalities, particularly amongst APOE-ε4 carriers. Our findings also confer biological validity to the construct of EYO as a potential stage marker of preclinical progression in the context of sporadic dementia. Further clinical follow-up of our longitudinal sample would provide critical validation of these findings.

1. Introduction

It is now established from clinicopathological and *in vivo* imaging studies that the neuropathological process of Alzheimer's disease (AD) and dementia begins decades before the earliest manifestation of cognitive or behavioural symptoms (Ritchie et al., 2016). A greater understanding of brain alterations occurring in the preclinical phase might identify novel biomarkers, aid earlier detection and assist in establishing treatment targets for AD. One approach to delineate early alterations is to evaluate longitudinal *in vivo* neuroimaging markers in asymptomatic individuals who are at increased risk for developing dementia.

Parental family history of dementia (FH+) is a recognised risk factor linked with increased cumulative lifetime risk for dementia, earlier age of onset as well as cognitive impairment (Scarabino et al., 2016). Previous neuroimaging studies have hinted at the presence of brain abnor-

* Corresponding author.
E-mail address: fkm24@medschl.cam.ac.uk (E. Mak).
[1] Joint first authorships.
[2] Joint senior authors.

https://doi.org/10.1016/j.neuroimage.2021.117749
Received 31 July 2020; Received in revised form 22 December 2020; Accepted 8 January 2021
Available online 14 January 2021

malities in FH+ individuals, such as reduced functional connectivity, hypoperfusion and grey matter atrophy (Adluru et al., 2014; Honea et al., 2010). However, our systematic reviews of structural and functional imaging studies in preclinical dementia have highlighted numerous discordant findings in the literature (Habib et al., 2017; Mak et al., 2017). Methodological differences, study designs and different age ranges are all plausible explanations for the discrepancy of findings in the FH literature. Yet an alternative possibility is that the presence of brain abnormalities may only be reliably detected amongst individuals who are on the precipice of symptom onset. Indeed, studies in cohorts of persons with familial AD mutations have proposed the estimated years to onset (EYO) as a stage marker of preclinical severity (Bateman et al., 2012). By exploiting the near certainty of dementia onset in carriers of familial AD mutations, EYO has been derived based on the difference between an individual's age and the parental age of symptom onset. Its association with deficits in functional connectivity (Ringman et al., 2011), alterations in white matter tracts (Ringman et al., 2007), white matter lesions (Viqar et al., 2015) and grey matter atrophy (Cash et al., 2013) has been investigated. A brief summary of key imaging findings on familial AD mutation carriers in relation to EYO is shown in Supplementary Table 1.

Data from the Swedish Twin Registry has demonstrated a strong heritable component of AD for both men and women (Gatz et al., 2006; Pedersen et al., 2004). A previous study also showed that heritable factors were associated with intergenerational age of symptom onset (Day et al., 2019). Collectively, these lines of evidence imply that EYO may be generalizable to some extent in sporadic AD and thus represents a surrogate index of preclinical disease progression. Our group first extrapolated the construct of EYO to a longitudinal cohort of cognitively normal midlife adults and found that FH+ individuals with a shorter EYO had worse visual working memory scores (Ritchie et al., 2017). Recent reports from an 'at risk' cohort have revealed that EYO was associated with temporo-parietal brain atrophy (Vogel *et al.*, 2018) and lower levels of cerebrospinal fluid (CSF) Aβ1-42, particularly amongst APOE-ε4 carriers (Villeneuve et al., 2018). Nevertheless, the mean age of their cohort was 63 years, and consequently the mean EYO was shorter (11 years to onset) relative to our sample in the PREVENT-Dementia study (Ritchie et al., 2013, 2017).

To extend previous cross-sectional studies (Caballero et al., 2018; Villeneuve et al., 2018; Vogel et al., 2018) and address the current gaps in our understanding of brain changes occurring during the preclinical stages, we mapped out an in-depth characterisation of EYO-related changes in (1) grey matter, (2) white matter microstructure, (3) white matter lesions, and (4) cerebral perfusion in a longitudinal cohort of FH+ individuals (mean follow-up of 2 years). We tested the hypotheses that individuals approaching their parental age of dementia diagnosis would show more severe deficits on multi-modal neuroimaging measures, expressed by a lower FA, higher MD and RD, more severe burden of white matter lesions, cortical and hippocampal atrophy, as well as reduced cerebral perfusion.

2. Materials and methods

2.1. Participants and clinical data

The protocol for the PREVENT study has been described in detail previously (Ritchie and Ritchie, 2012). Participants aged 40 to 59 years old with or without a parent with dementia were recruited through multiple sources, such as the register database held at West London Mental Health National Health Service Trust, part of the UK National Health Service. Other participants were recruited via the Join Dementia Research website through information about the study on the Internet and public presentations. Consented participants were seen at the West London Cognitive Disorders Treatment and Research Unit, West London Mental Health NHS Trust, where they were given a standardised neuropsychiatric interview and life-style questionnaires. Cognitive assessments were performed with the Addenbrooke's Cognitive Examination (ACE-III) during the follow-up visit. Blood was taken for APOE-ε4 genotyping with all members of the research and clinical teams remaining blind to the results.

2.2. Ethics statement

Approval for the study has been given by the NHS Research Ethics Committee London Camberwell St-Giles. EYO was estimated as the difference between the age of the participant and the age of dementia diagnosis of the earliest affected parent (if more than one parent had dementia) (Ritchie et al., 2017). Global cognition and domain-specific cognition was also evaluated using the Addenbrooke's Cognitive Examination (ACE-III) at Visit 2.

2.3. Multi-modal imaging acquisition

All subjects were scanned using a 3T Siemens Verio scanner. The following MR scans were acquired: A 3D T1-weighted magnetization prepared rapid gradient-echo (MPRAGE) image (TR = 2.3 s, TE = 2.98 ms, 160 slices, flip angle = 9°, voxel size = 1 mm^3 isotropic); a diffusion weighted image (DWI) with 64 directions (b = 1000 s/mm^2) in addition to a single non-diffusion weighted volume (TR = 11.7 s, TE = 90 ms, 63 slices, voxel size = 2 × 2 × 2 mm, flip angle = 90°); a Fluid-attenuated inversion recovery (FLAIR) scan (TR = 9 s; TE = 94 ms, 27 slices, voxel size=0.4 × 0.4 × 4 mm, TI = 2500 ms; flip angle = 150°) and an arterial spin labelling (ASL) dataset (PICORE Q2TIPS, 50 pairs of control/tag images, one calibration image, TR = 2.5 s / TE = 11 ms, inversion time = 1.8 s, bolus duration = 700 ms, voxel size 3.0 × 3.0 × 6.0 mm, 14 slices, flip angle = 90°). Details about the number of utilised scans per modality can be found in Supplementary Fig. 1.

2.4. Image preprocessing

2.4.1. Cortical thickness

The T1-MPRAGE scans were analysed using the automated longitudinal stream of Freesurfer version 6.0 (http://surfer.nmr.mgh.harvard.edu/) pipeline. The full details have been previously described (Reuter et al., 2012, 2010). Briefly, the pipeline applies motion correction, skull stripping, correction for field inhomogeneities, registration to and from the Talairach coordinate space, cortical parcellation and subcortical structure segmentation (Fischl, 2012). Three subjects were excluded due to failure of preprocessing steps of the Freesurfer recon-all pipeline (i.e. excessive misclassification of pial and white matter surfaces or severe skull stripping errors).

2.4.2. MNI normalisation

The individual T1-MPRAGE images were segmented with SPM12 to generate grey matter, white matter and CSF tissue probability maps. The generated grey matter images were inspected and when necessary manually corrected when parts of dura or residual skull were erroneously included in the grey matter cluster. Subsequently, the DARTEL pipeline was used to create a study specific template based on the grey and white matter masks from both study time-points. DARTEL makes use of non-linear diffeomorphic registration to register individual grey matter masks to the study-specific template and subsequently an affine registration to register the study specific template to the MNI space (Ashburner, 2007). The derived flow fields were used in the subsequent analyses to spatially normalise the T1 MRI to the MNI space. The grey matter mask for subsequent analyses was derived from the average grey matter maps and thresholded at 25% probability.

2.4.3. Perfusion measures

ASL post-processing was performed using FSL's Bayesian Inference for ASL MRI (BASIL) toolbox (Chappell et al., 2009). The acquired ASL

scans were motion corrected using FSL's MCFLIRT and calibrated based on a proton density acquisition. Spatial regularization was applied prior to cerebral blood flow (CBF) calculation. CBF was quantified using the Buxton ASL kinetic model (Buxton et al., 1998) according to the model suggested in the ASL white paper (Alsop et al., 2015). The generated CBF images were corrected for the presence of partial volume effects using FSL BASIL's adaptive spatial prior approach (Chappell et al., 2011). To proceed to partial volume correction (PVC), the MPRAGE images were registered to the ASL calibration scan using FSL's FLIRT. The same transformation was applied to coregister the high-resolution partial volume maps to the ASL resolution. PVC grey matter perfusion maps and grey matter CBF mean values were recorded for voxels with grey matter > 10%. Subsequently, the grey matter CBF maps were registered to the T1 images using the inverse transform generated in the previous step and normalized to the MNI space using SPM's DARTEL. To proceed to voxelwise comparisons a grey matter CBF mask was created for each subject including voxels with at least 5 ml/100 g/min. All individual masks were summed up and a threshold of 95% was used for voxel retention. Finally, this mask was multiplied by the grey matter mask generated in the previous step. Consistent with previous methodology (Dolui et al., 2017), the temporal SNR (tSNR) of the ASL acquisition was determined as follows: the time-series were motion corrected using FSL MCFLIRT. Subsequently, individual perfusion weighted images (control-labelled) were generated for all 50 repetitions. A mean value for each of the 50 perfusion weighted images within areas of grey matter >10% was calculated, and tSNR was measured as the mean over the standard deviation of these values (2.11 ± 0.9).

2.4.4. White matter microstructure

The diffusion datasets were visually inspected for optimal coverage and to ensure minimal eddy-current distortions by 2 authors (EM and EMK). 9 subjects were excluded due to excessive EPI distortions, while 1 subject was excluded due to poor field-of-view coverage. DWI data were stripped of nonbrain tissue using the Brain Extraction Tool (BET). Eddy currents and head movements were corrected with "eddy" in FSL (Version 6.0.1). Quantitative identification of slices with signal loss was performed in "eddy" and these volumes were replaced by non-parametric predictions using the Gaussian process (Andersson et al., 2016). In addition, we also corrected for intra-volume movement (Andersson et al., 2017). The b-matrix was subsequently reoriented by applying the rotational part of the affine transformation used during eddy correction (Leemans and Jones, 2009). Diffusion tensors were generated from the eddy-corrected DWI datasets using DTIFIT in FSL 6.0.1. We pursued an unbiased longitudinal approach for the spatial normalisation of diffusion datasets using the Diffusion Tensor Imaging Toolkit (DTI-TK). Firstly, tensor images at baseline and follow-up were created by converting the diffusion eigenvectors and eigenvalues using the function fsl_to_dtitk in DTI-TK. Secondly, for each participant, an unbiased intra-subject template was generated using the tensor datasets from his or her baseline and follow-up after an iterative process of rigid, affine and non-linear diffeomorphic registrations. Next, the within-subject templates were used to create a study-specific population template using the same iterative process. Each participant's DWI data was normalised to the group-specific template via a single interpolation step. Fractional anisotropy (FA), mean diffusivity (MD) and radial diffusivity (RD) maps were generated using the normalised tensor images. Following the tensor-based registration, a mean FA map was derived from the group template and skeletonised using *tbss_skeleton* in FSL to create the mean FA skeleton (thresholded at FA > 0.2). FA, MD and RD images from each participant were projected onto the mean FA skeleton by searching for maximum FA values perpendicular to the skeleton. To complement our voxel-wise analyses, mean global FA, RD and MD values were extracted at baseline and follow-up from each participant's white matter skeleton using the *fslmaths* command.

2.4.5. Quantification of WMH

WMH lesion maps were obtained using an automated script on the Statistical Parametric Mapping 8 (SPM8) suite (http://www.fil.ion.ucl.ac.uk/spm/) on FLAIR MRI; details on the procedures involved have been described previously (Firbank et al., 2003; Smart et al., 2011). All lesion maps from both baseline and follow-up visits were reviewed by a single experienced rater (A.L.) while blinded to all clinical information. Lesion maps obtained from the segmentation procedure were used as starting points for manual WMH delineation. Baseline and follow-up FLAIR images were evaluated side by side during delineation to ensure consistency. WMH volumes were normalised by total intracranial volume to account for individual differences in head size. To generate a descriptive voxelwise map representing the spatial topography of WMH occurrence in our sample, we normalised the binarized lesion maps to the MNI152 template using the forward transformations from T1-MPRAGE to MNI152 space. Next, the normalised lesion maps were concatenated using *fslmaths*. A mean image was created to represent the lesion probability map, in which the intensity of each voxel represents the likelihood of WMH occurrence across our sample.

2.5. Statistical analyses

A summary of the key imaging outcomes is illustrated in Fig. 1. To characterise brain imaging changes in relation to EYO, we used all available longitudinal datasets for all participants. Demographic variables were compared between the APOE-ε4 groups using *t*-tests, Wilcoxon Rank sum tests, chi-square tests where appropriate. To increase robustness of our correlations, EYO was transformed with the inverse normal transformation due its skewed distribution, increasing the robustness of correlations (Miller et al., 2016). Voxelwise associations of EYO with imaging changes were investigated using the longitudinal Sandwich Estimator (SwE) toolbox (http://www.nisox.org/Software/SwE) (Guillaume et al., 2013). This marginal model describes expected variability as a function of predictors in a design matrix, while additionally accounting for correlations due to repeated measurements and unexplained variations across individuals. The main models featured the main effects of EYO as well as its interactions with time (i.e. centred within-subject age of participant). The latter metric allowed us to assess whether a hypothetical proximity to dementia may have an accelerating effect of imaging changes over time, while the main effect of EYO indicates whether a hypothetical proximity to dementia is related to imaging differences across the sample, independent of other covariates. The covariates included are (i) the demeaned mean age of a subject over both time points, (ii) the demeaned quadratic term of age to account for potential non-linear age associations (Kodiweera et al., 2016; Salami et al., 2012), (iii) sex, (iv) demeaned years of formal education and time. The demeaned average WMH volume and its interaction with time were included as additional covariates in all DTI analyses to ensure that white matter changes are not confounded by small vessel disease. In addition, we examined both potential moderating and interactive effects of APOE-ε4 by modelling the main effects of APOE-ε4 and its interactions with EYO and time into the SwE models. Non-parametric statistical inference was based on the Wild Bootstrap procedure (Guillaume et al., 2015), and corrections for multiple comparisons were performed with Threshold-Free Cluster Enhancement (TFCE) and Family-Wise Error Rate (TFCE $P_{FWER} < 0.05$) (Smith and Nichols, 2009). To report the coordinates of significant clusters in standard MNI152 space, the mean FA of the group-specific template was affine registered to the MNI152 atlas using FLIRT and visually inspected. The affine transformation was then applied onto the statistical maps for anatomical localisations in MNI152 space. To eliminate noise due to averaging and normalization, significant clusters with < 50 voxels were excluded from the table of results. Non-voxelwise analyses of global FA, MD, RD, mean grey matter perfusion, and mean cortical thickness were performed using Linear Mixed Effect models (LME), implemented with the *lmer* function of the lme4

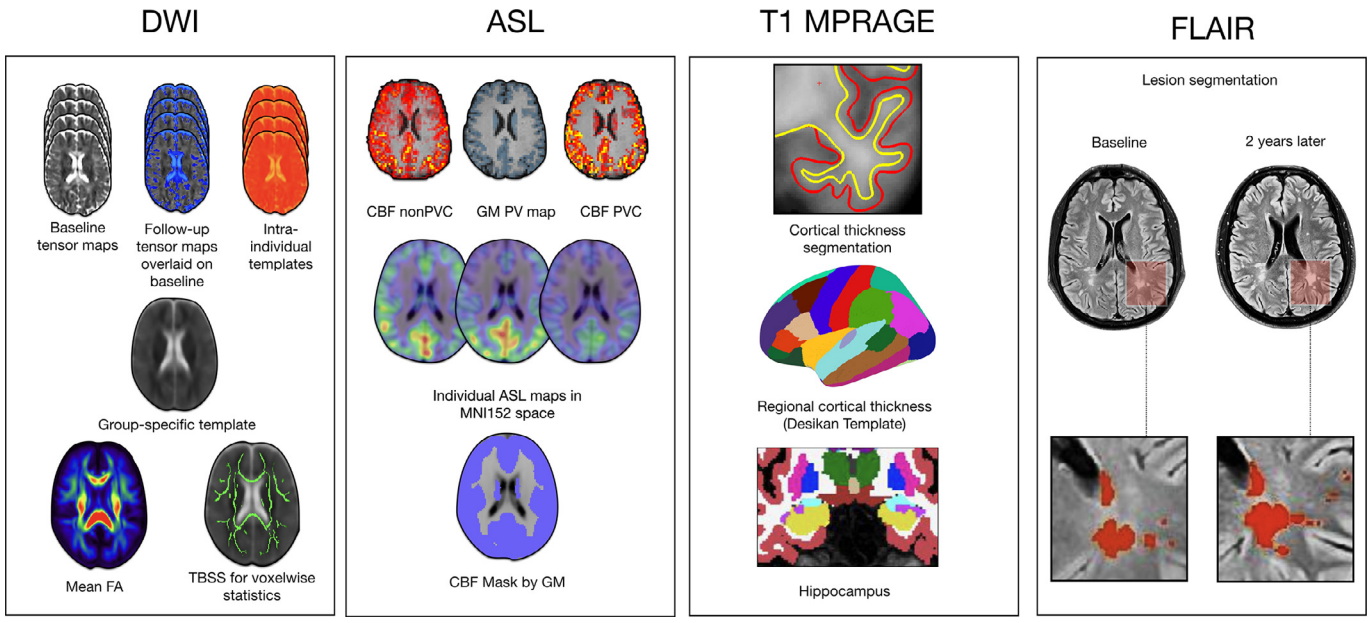

Fig. 1. Multi-modal neuroimaging outcome measures at both baseline and follow-up. Global FA, MD and RD were estimated using DTI-TK after generating a group-specific template that was unbiased to both time-points. T1-MPRAGE datasets were processed using Freesurfer for the segmentations of cortical thickness and hippocampus. ASL data were processed using FSL-BASIL, co-registered to the T1-MPRAGE, and visually inspected by 2 independent operators for errors in alignment. Grey matter perfusion was quantified following PVC of the CBF maps using the grey matter mask. WMHs were segmented from FLAIR data. Abbreviations: FA = Fractional Anisotropy, MD = Mean Diffusivity, RD = Radial diffusivity, DTI-TK = Diffusion Tensor Imaging Toolkit, AD = Alzheimer's disease, ROI = Regions of Interests, ASL = Arterial Spin Labelling, WMHs = White matter hyperintensities; PVC = Partial Volume Corrected; CBF = Cerebral Blood Flow.

package in R (Bates et al., 2015). Consistent with our SwE models, the LME models included a random intercept for each subject, and fixed effects of demeaned averaged age, demeaned quadratic age, sex, demeaned years of education and time (i.e. the demeaned within-subject age). WMH volumes were also included as additional covariates in our analyses on FA, MD and RD.

As the EYO was derived based on the participant's age, both measures were expected to be correlated ($r = -0.3$, $p < 0.01$; Supplementary Fig. 2). We also took extra caution to verify the absence of multicollinearity in our models by calculating variance inflation factors (VIF) using the *CAR* package (Fox and Monette, 1992; Fox and Weisberg, 2019). Finally, two sets of sensitivity analyses were conducted to examine the robustness of the significant EYO associations against chronological age. First, we repeated all significant LME and SwE models while substituting the EYO variable with age. Secondly, to compare the relative contributions of age, EYO and APOE-ε4 status on imaging changes, we conducted group comparisons of imaging data between median-split age groups, median-split EYO groups, and APOE-ε4 status using ANCOVA.

2.6. Data availability

Data will be made available upon reasonable requests and for non-commercial reasons. The statistical maps, group templates and other relevant files are available to view on Neurovault (https://identifiers.org/neurovault.collection:9099).

3. Results

3.1. Sample characteristics

Demographic details about the sample with diffusion imaging datasets are summarised in Table 1. The EYO ranged from 38 years before the parental onset to −3 years after onset. There were no significant differences with regards to age, gender, education years or ACER between the APOE-ε4 carriers and non-carriers.

Table 1
Participant characteristics of subjects with diffusion weighted imaging datasets.

	APOE-ε4 − (*N*=42)	APOE-ε4 + (*N*=37)	*P*-value
Age (years)			
Mean (SD)	53.4 (4.34)	51.8 (4.83)	0.086
Median [Min, Max]	54.0 [41.0, 60.0]	52.0 [40.0, 60.0]	
Gender			
Female	31 (73.8%)	27 (73.0%)	0.99
Male	11 (26.2%)	10 (27.0%)	
Education (years)			
Mean (SD)	15.7 (2.92)	15.7 (3.12)	0.561
Median [Min, Max]	16.0 [11.0, 22.0]	17.0 [11.0, 21.0]	
ACE-III			
Mean (SD)	94.3 (4.73)	95.1 (3.93)	0.644
Median [Min, Max]	95.0 [80.0, 100]	97.0 [82.0, 100]	
Missing	2 (4.8%)	0 (0%)	
ACE-III Memory			
Mean (SD)	24.6 (2.07)	24.8 (1.91)	0.974
Median [Min, Max]	26.0 [18.0, 26.0]	25.0 [18.0, 26.0]	
Missing	2 (4.8%)	0 (0%)	
Time interval (years)			
Mean (SD)	2.00 (0.122)	2.01 (0.131)	0.957
Median [Min, Max]	2.00 [1.72, 2.32]	1.98 [1.86, 2.46]	
EYO (years)			
Mean (SD)	24.6 (6.73)	23.5 (7.86)	0.345
Median [Min, Max]	26.0 [4.00, 33.0]	25.0 [-3.00, 38.0]	

Abbreviations: ACE-III = Addenbrooke's Cognitive Examination, EYO = Estimated years to onset.

3.2. Reliability of imaging data across time

The *sjstats* package in R was used to calculate the intra class coefficients. ICC was calculated as the proportion of between-subject variance to total variance. The dependent variable for these models was the global imaging measurement for each subject on two separate visits, fixed effects included the average age and time. Subject-specific intercept was included as a random effect. Across all imaging measurements,

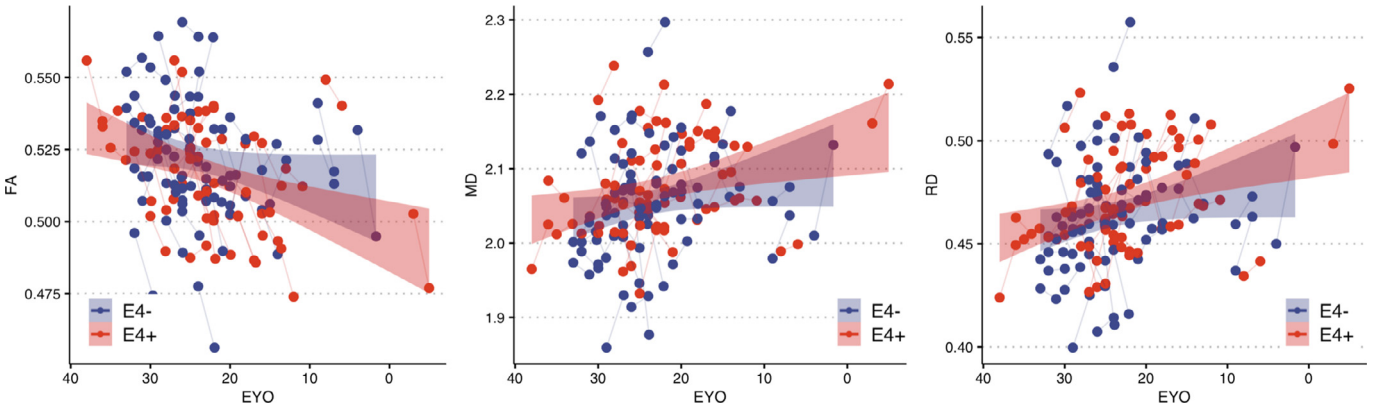

Fig. 2. Linear mixed effect modelling of global white matter microstructure in relation to EYO. Lower FA, and higher MD and RD values were associated with nearer proximity to hypothetical age of onset of dementia in FH+, after adjusting for averaged age, age^2, gender, education years, averaged WMH volume, APOE-ε4 status, and time (i.e. demeaned within-subject age). 95% confidence intervals are illustrated by the blue and red boundaries in non-carriers and APOE-ε4 carriers respectively.

ICC was moderate to excellent [Mean cortical thickness: 0.87, FA: 0.73, MD: 0.74; RD: 0.74; ASL: 0.55].

3.3. Grey matter atrophy

There were no significant main effects of EYO on regional cortical thickness and hippocampal volumes that survived false discovery rate correction for multiple comparisons. No regions showed a significant interaction between EYO × APOE4 status, or three-way interactions between EYO × Time × APOE4 status after false discovery rate correction for multiple comparisons.

3.4. White matter microstructural changes

The association between white mater changes and EYO are illustrated in Fig. 2. There were no significant effects of APOE-ε4 status on white matter changes in terms of FA ($T = -1.13$, $p = 0.26$), MD ($T = 1.11$, $p = 0.27$) or RD ($T = 1.16$, $p = 0.25$). LME models showed significant main effects of EYO on FA ($T = 2.58$, $p = 0.01$), MD ($T = -2.55$, $p = 0.01$) and RD ($T = -2.66$, $p = 0.01$). There were no significant interactions between time and EYO ($T = -1.12$–1.43, $p = 0.16$–0.43). Voxelwise SwE revealed widespread and significant main effects of EYO on FA, MD, and RD maps, after adjusting for averaged age, age^2, gender, education years, averaged white matter hyperintensity volume, APOE-ε4 status, and within-subject age (TFCE $_{FWER}$ $p < 0.05$). The EYO-associated white matter changes were predominantly found in the forceps minor of the corpus callosum, inferior longitudinal fasciculi, superior longitudinal fasciculi, cingulum bundles, anterior thalamic radiation, inferior fronto-occipital fasciculus, uncinate fasciculus (see Supplementary Table 3 for MNI152 coordinates of peak clusters).

3.5. White matter hyperintensities

We illustrated the baseline WMH incidence, voxel-wise, across our sample and revealed the expected spatial distribution of WMHs in normal ageing (Fig. 4). The highest probabilities of WMH were concentrated around the periventricular areas and in deep white matter regions. There were no significant main effects of EYO ($T = -0.74$, $p = 0.46$) or EYO – Time interactions ($T = -1.06$, $p = 0.29$) on WMH volumes.

3.6. Cerebral perfusion

LME and SwE voxel-wise analyses revealed a significant interaction of EYO with APOE-ε4 on grey matter perfusion (LME: $T = -2.87$; $p = 0.01$; SwE: TFCE $_{FWER}$ $p < 0.05$) such that APOE-ε4 carriers showed increased perfusion with nearer proximity to onset while APOE-ε4 non-carriers did not (Fig. 5). The difference in effects between APOE-ε4 carriers and non-carriers was qualified by a significant interaction term (LME: $T = -2.87$; $p = 0.01$). Simple slope analyses and slope difference tests further confirmed a significant difference in the relationship between EYO and ASL for the APOE-ε4 carriers and non-carriers, such that a significant association was found only amongst the APOE-ε4 carriers (Slope analysis: $T = -3.27$; $p < 0.01$) and not for the non-carriers (Slope analysis: $T = 0.74$; $p = 0.462$). Similarly, SwE voxelwise analyses revealed that the EYO × APOE-ε4 interaction was localised within temporo-parietal regions, such as the hippocampus, precuneus/posterior cingulate cortices (TFCE $_{FWER}$ $p < 0.05$; see Supplementary Table 4 for MNI152 coordinates of peak clusters). There were no significant three-way interactions between EYO, APOE-ε4 and time.

3.7. Cross-modal relationships between ASL and DTI data

Scatter plots of the relationships between grey matter perfusion and DWI metrics are shown in Fig. 6. Post-hoc robust linear regressions indicated a significant negative correlation of FA ($T = -2.95$, $p < 0.01$) and positive correlations of MD ($T = 2.29$, $p = 0.03$), and RD ($T = 2.66$, $p = 0.01$) with grey matter perfusion after adjusting for age, age^2, gender, education years, APOE-ε4 status, and WMH volumes.

3.8. Sensitivity analyses

3.8.1. Substituting EYO with age

Given that age is correlated with EYO, we performed two sets of sensitivity analyses to evaluate the age-independence of the EYO results. First, the EYO term was substituted by the chronological age of the participant. These analyses are informative in terms of showing whether the spatial extent of proximity-related white matter changes could be recapitulated from the participant's age itself. First, age was not significantly correlated with global mean FA ($T = -1.88$, $p = 0.06$), MD ($T = 1.31$, $p = 0.19$) or RD ($T = 1.64$, $p = 0.11$). Akaike Information Criteria analysis also indicated that including EYO resulted in a better model fit compared to a reduced model with age alone ($p = 0.007$). Second, in our voxelwise SwE models without the EYO term, older age was only associated with lower FA but not MD or RD (TFCE$_{FWER}$ $p < 0.05$). The spatial extent of the age-FA associations was markedly smaller to that of the EYO (Dice volume overlap = 17.4%). The voxels that are unique to either EYO, age, or overlapping effects are illustrated in Fig. 7, showing that EYO is sensitive to microstructural changes over and beyond that of normal ageing. Similarly, in contrast to EYO, there was no

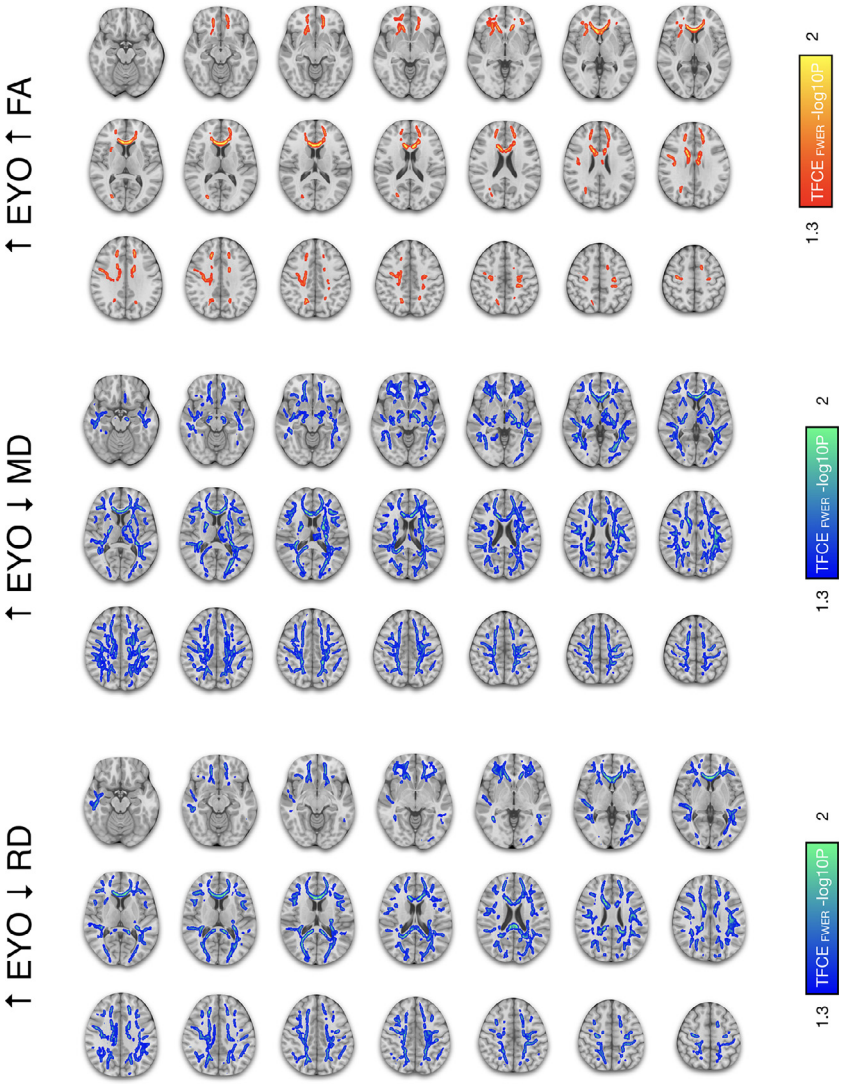

Fig. 3. Sandwich estimator voxel-wise modelling of white matter microstructural changes in relation to EYO. Widespread extent of decreased FA, increased MD and RD were associated with nearer proximity to hypothetical age of onset of dementia in FH+. Images are shown in radiological convention. Abbreviations: EYO = Estimated years to onset of dementia, FA = Fractional anisotropy, MD = Mean diffusivity, RD = Radial diffusivity; TFCE = Threshold Free Cluster Enhancement, FWER = Family wise error rate.

significant interaction between age and APOE-ε4 status on mean grey matter perfusion ($T = 0.46$, $p = 0.65$).

3.8.2. *Group comparisons of white matter across binarized subgroups*

We also attempted to disentangle the contributions of ageing, APOE-ε4 and EYO through a series of group comparisons (Figure 8). The dependent variable was the imaging metric at baseline (i.e. FA). The categorical covariates are age groups (Age ≥ 53 and Age < 53), APOE4 (Carriers and Non-Carriers), and EYO proximity groups (EYO ≥ 25 and EYO < 25). WMH volumes were also included to account for white matter alterations due to small vessel diseases. This parsimonious stratification of the sample enabled a comparison of the relative impact of each risk factor on imaging changes. ANOVA indicated a significant main effect that was exclusive to EYO ($F = 6.52$, $p = 0.01$). Furthermore, the effect size was the largest for EYO (Cohen $f = 0.3$) relative to age (Cohen $f = 0.06$) and APOE-ε4 (Cohen $f = 0.09$). The predominant effect of EYO was also evident in MD and RD analyses.

4. Discussion

Our study revealed an assortment of brain changes as cognitively normal FH+ individuals approach their expected onset of dementia in midlife. A shorter hypothetical proximity to dementia was associated with widespread white matter disruption (↓ FA ↑ MD ↑ RD), in the absence of grey matter atrophy. In addition, Moreover, our data showed that hyperperfusion with shorter EYO was strongly predicated on the presence of APOE-ε4 status.

We did not find a robust effect of EYO on regional grey matter atrophy. This finding was not entirely unexpected, as cortical atrophy detected on MRI is widely believed to represent the terminal end-product of neuronal loss, cell shrinkage, reductions in dendritic extent and synaptic loss (McEwen, 1997). In contrast, extensive white matter deficits were revealed as FH+ individuals approached their estimated age of onset, involving major white matter bundles that are characteristically compromised in mild cognitive impairment and AD (Acosta-Cabronero et al., 2010). Cross-sectional studies in late-onset AD and familial AD have demonstrated preferential vulnerability of the corpus callosum, the superior and inferior longitudinal fasciculus, and cingulum bundles of the limbic projections, and our findings extend those reports by documenting a similar profile of white matter degeneration in a cognitively normal cohort of midlife adults. To the extent that EYO is a valid stage marker of preclinical disease progression, it is conceivable that the pattern of white matter deficits in our data may reflect incipient neuropathologies (i.e. amyloid or early build-up of neurofibrillary tau tangles). While the EYO correlations preclude causal interpretations, our hypothesis is aligned with a recent study that included both ante-mortem DTI and histological analyses in cognitively normal subjects (Kantarci et al., 2017). In that study, Kantarci et al., demonstrated associations of temporo-parietal white matter tracts with amyloid burden and tau accumulation (Kantarci et al., 2017). Despite the lack of a

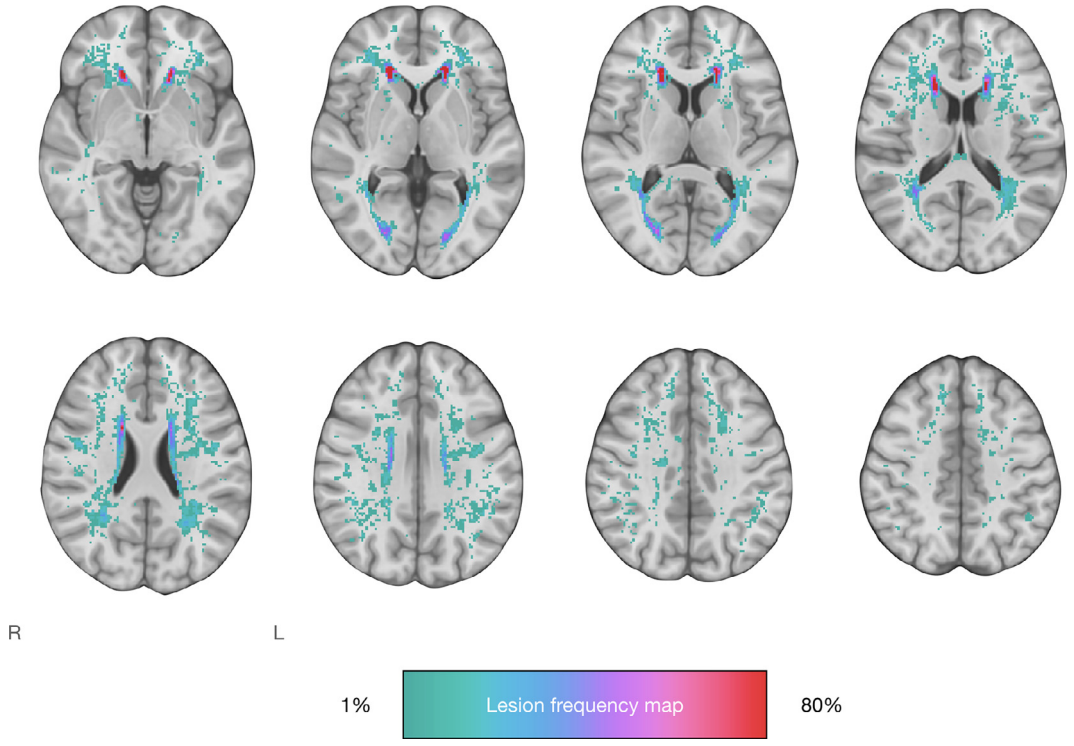

Fig. 4. Frequency maps of WMH distribution in our sample. Axial views demonstrate the mean pattern of WMH in our sample, overlaid on the T1-MNI152 template. The percentage of lesion probability is indicated by the colour bar. Abbreviation: WMH = White matter hyperintensities.

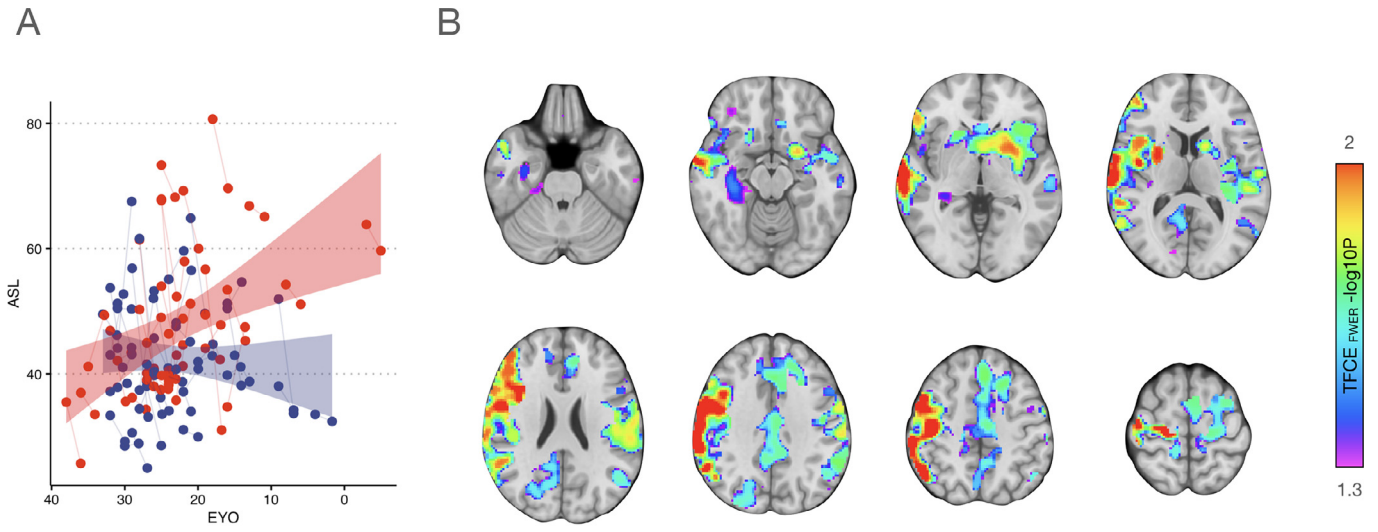

Fig. 5. Associations of EYO with cerebral perfusion changes. A: After adjusting for averaged age, age^2, gender, education years, and time, there was a significant EYO × APOE-ε4 interaction, indicating a pattern of hyperperfusion as APOE-ε4 carriers approached the hypothetical age of onset of dementia. 95% confidence intervals are illustrated by the blue and red boundaries in non-carriers and APOE-ε4 carriers respectively. B: SwE voxel-wise modelling of EYO x APOE-ε4 interactions on cerebral perfusion. Images are shown in radiological convention. Abbreviation: EYO = Estimated years to onset of dementia; FH+ = Individuals with a family history of dementia, ASL = Arterial Spin Labelling, TFCE = Threshold Free Cluster Enhancement, FWER = Family wise error rate; SwE = Sandwich Estimator.

prior finding in the FH+ literature, our findings are corroborated by recent data from the Dominantly Inherited Alzheimer's Network (DIAN) project, which found elevated MD with shorter EYO (Caballero et al., 2018). Interestingly, there were pronounced EYO-related changes in the genu of the corpus callosum, coinciding with the striking convergence of proximity-related FA, MD, and RD changes in our sample (Fig. 3).

In contrast to the anticipated trajectory of ↓ FA ↑ MD ↑ RD on white matter tracts, a shorter EYO was accompanied by *increased* perfusion particularly amongst APOE-ε4 carriers. Hyperperfused regions encompassed the temporo-parietal regions (i.e. precuneus, posterior cingulate, medial temporal regions and hippocampus). At first glance, these results may appear to contradict the wealth of evidence showing ~40% global deficit of CBF in people with AD in the same aforementioned regions (Alsop et al., 2010; Wierenga et al., 2014). However, our data are also aligned with other reports of hyperperfusion amongst APOE-ε4 carriers (Bangen et al., 2012; Wierenga et al., 2013): increased glucose uptake from FDG-PET studies have been found in FAD mutation carriers as early as 25 years before expected onset (Benzinger et al., 2013)

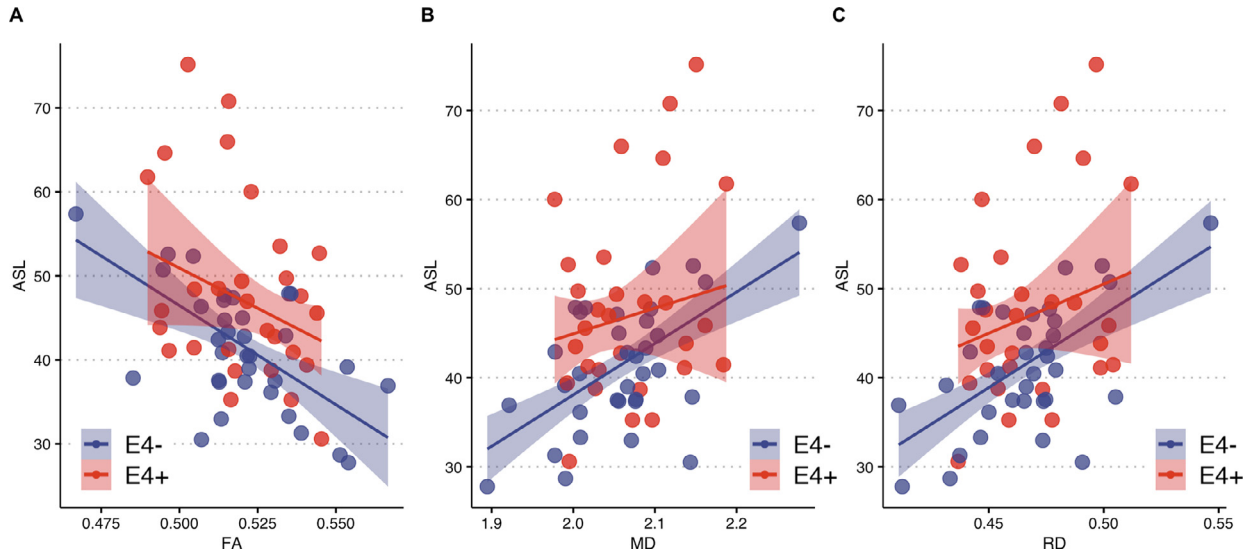

Fig. 6. Scatter plots of the associations between grey matter perfusion and global white matter indices. 95% confidence intervals are illustrated by the green and purple boundaries in non-carriers and APOE-ε4 carriers respectively. Abbreviation: FH+ = Individuals with a family history of dementia; FA = Fractional anisotropy, MD = Mean diffusivity, RD = Radial diffusivity.

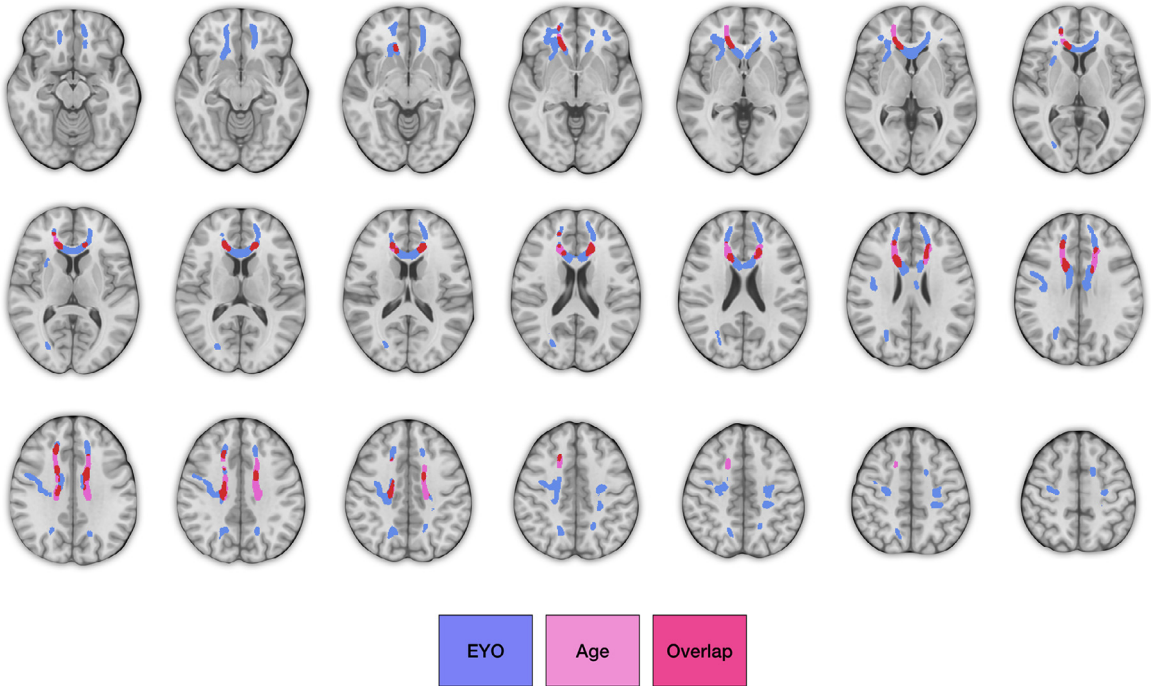

Fig. 7. Comparing the spatial extent of FA changes with age and EYO. Binarised maps of the TFCE corrected maps are shown. Older age correlated with FA reductions primarily in the corpus callosum, whereas EYO was associated with a broader extent of FA reductions that encompassed the corpus callosum, inferior and superior longitudinal fasciculus, cingulum, inferior fronto-occipital fasciculus and corticospinal tract. Abbreviations: EYO = Estimated years to onset of dementia, FA = Fractional anisotropy. TFCE = Threshold Free Cluster Enhancement, FWER = Family wise error rate.

while Alsop et al. have reported hippocampal hyper-perfusion in cases with AD (Alsop et al., 2008). Taken together, our current perfusion data are consistent with a model of disease progression in the asymptomatic period of dementia, in which APOE-ε4 carriers display elevated cerebral perfusion very early during the presymptomatic phase as a possible attempt to maintain an adequate blood supply at rest. Hyperperfusion could also be a response to neuroinflammation (Alsop et al., 2008), alterations in the capillary transit time (Østergaard et al., 2013) or associated with amyloid accumulation (Fazlollahi et al., 2020). Another possible explanation is that the higher ASL signal is driven by delayed intravascular signal. However, our subjects were all healthy participants hence we do not expect large differences in the arterial transit time. The inversion time used in our protocol is also aligned with previous recommendations (Alsop et al., 2015). In a study by Wierenga et al. (2013) the interaction of age and APOE-ε4 was investigated in relation to CBF and it was found that young APOE-ε4 (mean age: 24) demonstrated hyperperfusion, whereas older APOE-ε4 carriers (mean age: 75) demonstrated hypo-perfusion compared to non-carriers. Some plausible explanations for the observed associations include the (a) uncoupling of the flow from metabolic demands in young adults, in turn leading to cerebrovas-

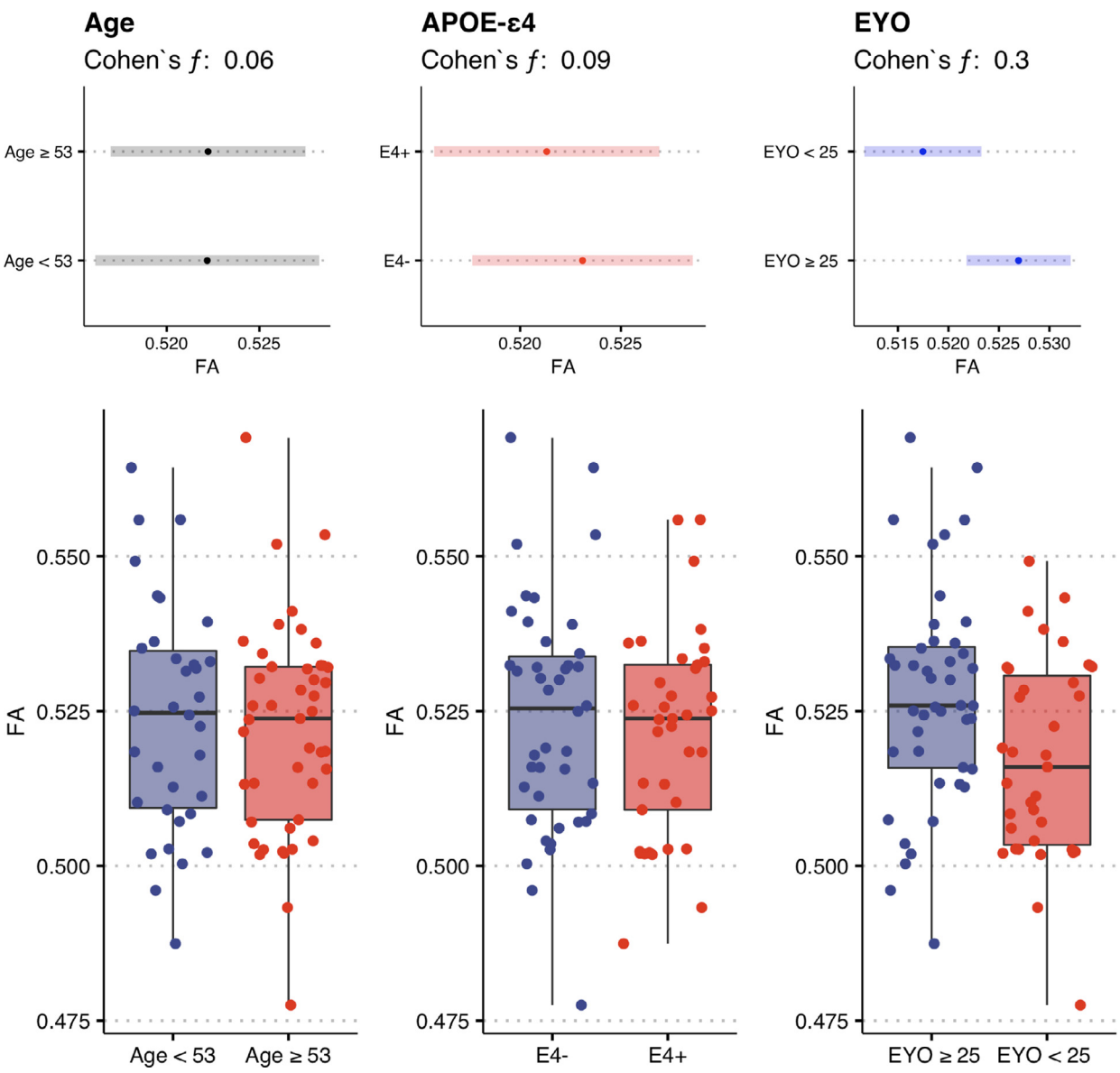

Fig. 8. Proximity to dementia is the predominant contributor to white matter changes compared to age and APOE-ε4 status. FH+ individuals who are less than 25 years to estimated onset showed significantly reduced white matter FA compared to FH+ individuals who are ≥ 25 years away from estimated onset. EYO group had the largest effect size relative to age group and APOE-ε4 status. Abbreviation: FA = Fractional Anisotropy, EYO = Estimated years to onset.

cular dysregulation, (b) a differential effect of APOE-ε4 on neurovascular function in aging, (c) and hypo-perfusion as a result of amyloid accumulation or even underlying structural alterations in the vasculature in older carriers. These hypotheses are especially pertinent to this study, considering the intermediate mean age of our cohort relative to the aforementioned age groups (Wierenga et al., 2013). Future studies with additional measurements of cerebral hemodynamics using arterial transit time sensitive ASL acquisitions or diffusion weighted ASL may be well-suited to reveal further insights into the hemodynamic changes and identify the inevitable inflection point associated with the emergence of the AD-signature pattern of hypoperfusion.

A key strength of the present study is the integration of multi-modal MR imaging, enabling several inferences regarding the evolution of distinct pathological mechanisms along the preclinical spectrum. First, the coupling of EYO with DTI instead of cortical thickness provides further support to the argument that microstructural changes – typically not visible on T1-MPRAGE – predate macroscale neurodegeneration/brain atrophy, and thus could predict subsequent cognitive decline with greater sensitivity (Kantarci et al., 2005; Müller et al., 2005; Ringman et al., 2007; Weston et al., 2015). Secondly, against the backdrop of widespread white matter degeneration, it is tempting to speculate that elevated perfusion may reflect the harnessing of greater neural resources to help circumvent the deteriorating efficiency of cognitive networks. There is some tangential support for this hypothesis from a recent study showing a paradoxical relationship between elevated cerebral perfusion and increased amyloid burden in a cognitively normal elderly cohort (Fazlollahi et al., 2020). Likewise, a compensatory hypothesis would have the corollary that elevated cerebral perfusion is accompanied by microstructural impairments (↓ FA ↑ MD ↑ RD), as was confirmed in our post-hoc cross-modal associations between DTI and ASL. Interestingly, a recent study found the inverse relationship in patients with chronic traumatic brain injury (TBI, but *not* in those with less remote TBI (Clark et al., 2017). Taken together, these findings provide preliminary evidence for a dynamic association between CBF and white matter integrity that may exert deleterious effects on cognitive outcomes.

Valid interpretations of the EYO × imaging associations are critically dependent on the removal of age-related confounds. As expected, there was a modest correlation of $R = -0.3$ in our study (Supplementary Fig. 2). While the narrow age range of our study may reduce the risk of spurious correlations between EYO and imaging findings, we undertook several analyses to ensure the robustness of the EYO findings against age. Firstly, our EYO findings remained significant after correcting for both the linear and quadratic terms of age in all analyses. Secondly, to assess the age-independence of the associations between EYO and imaging changes, we repeated our analyses by using age itself as the predictor of imaging changes in lieu of EYO. There were focal age-associated reductions in FA within the corpus callosum, in keeping with previous studies (Bennett et al., 2010; Salami et al., 2012). In contrast, the extensive associations of EYO with white matter deficits (↓ FA ↑ MD ↑ RD) are indicative of other mechanisms that are distinct from normal ageing. Indeed, future studies investigating CSF or PET biomarkers of [^{18}F]-AV1451 and [^{11}C]-PiB in relation to EYO would be imperative to delineate the pathological undercurrents of white matter dysfunction as individuals approach dementia onset.

Our findings should also be considered with several other caveats. WMHs may confound our interpretations of DTI findings. However, our cohort is one of the youngest in the prevailing literature, and as such would be expected to have less cerebrovascular pathology (Stefaniak et al., 2018). In addition, all DTI analyses were corrected for WMH volumes. The lack of associations between EYO and WMH could also be interpreted in the context of a previous study in FAD mutation carriers, which found an association between shorter EYO and more severe WMH only amongst individuals with autosomal dominant genetic mutations, whereas no such correlations were found amongst the non-carriers (Lee et al., 2016). Another limitation is that the utilised ASL acquisition did not allow for quantification of arterial transit time and the separation of arterial and tissue compartments. However, we do not anticipate large variability in arterial transit time given the inversion time of 1.8 s in our ASL protocol. The dominant model for perfusion quantification in ASL which was used in the present study, assumes instantaneous water exchange between the capillary and tissue compartments (Buxton et al., 1998). In the case of altered water exchange rates, utilization of a single-compartment model could potentially introduce bias in CBF quantification. It is still unclear the water exchange rate differs between APOE4 carriers and non-carriers, especially during the preclinical stage of the disease. In a recent study by Montagne et al., cognitively asymptomatic APOE4 carriers demonstrated a blood brain barrier breakdown compared to APOE3 carriers, however the examined cohort was more than 10 years older on average compared to the present study (Montagne et al., 2020). Future studies using novel ASL sequences capable of quantifying delays in the blood delivery to the tissue or changes in the water exchange rate could reveal more insights about neurovascular changes associated with preclinical dementia and EYO (Jezzard et al., 2018; Shao et al., 2019). Finally, despite a modest genetic influence on the age of onset of AD (Day et al., 2019), the EYO variable remains a hypothetical stage marker of subclinical disease progression and its utility for early diagnosis in sporadic dementia is still an open question. On this note, 1 subject had a negative EYO (i.e., older than his/her parental age of dementia). However, repeating the analyses without this subject did not influence our findings.

5. Conclusions

Building upon previous work of proximity-related brain changes in familial AD mutation carriers, the plethora of findings in this study provide compelling evidence that the preclinical phase of sporadic dementia is characterised by subtle microstructural and physiological cerebral abnormalities in the absence of grey matter atrophy. Crucially, we demonstrated that these changes are not simply a reflection of normal ageing, highlighting the estimated temporal proximity to dementia as a potential metric with valuable clinical relevance and prognostic utility. Further validation of the EYO in larger samples of cognitively normal APOE-ε4 carriers/FH+ is warranted and will be performed as more subjects in PREVENT-Dementia complete their follow-up assessments.

Credit author statement

EM and MD performed the imaging analysis, conducted the statistical analysis, and drafted the manuscript. GTM provided statistical advice and critical feedback on the manuscript. AL, SFC, EMK, GBW, PSJ, IC, KR, CR, LS and JOB reviewed and provided critical feedback on the manuscript. CR, JOB, LS also helped obtain funding, supervised this study, was involved with its design.

Data availability

Data will be made available upon reasonable requests and for non-commercial reasons. The statistical maps, group templates and other relevant files are available to view on Neurovault (https://identifiers.org/neurovault.collection:9099).

Financial disclosures

John T. O'Brien has no conflicts related to this study. Unrelated to this work he has received honoraria for work as DSMB chair or member for TauRx, Axon, Eisai, has acted as a consultant for Roche, has received research support from Alliance Medical and Merck. Elijah Mak, Maria-Eleni Dounavi, Stephen Carter, Audrey Low, Li Su, Elizabeth McKiernan, Karen Ritchie, Graciela Muniz, Isabelle Carriere, Guy Williams, Simon Jones and Craig Ritchie have no conflicts of interest to declare.

Acknowledgements

Participants were recruited at West London Mental Health National Health Service (NHS) Trust (now known as West London NHS Trust) and scanning was carried out at the Clinical Imaging Facility, Imperial College London. We thank all the PREVENT-Dementia participants for their enthusiastic participation in this study. Infrastructure support was provided by the High Performance Hubs for Clinical Informatics (HPHI), funded by the MRC Research Infrastructure Award (MR/M009041/1).

Supplementary materials

Supplementary material associated with this article can be found, in the online version, at doi:10.1016/j.neuroimage.2021.117749.

References

Acosta-Cabronero, J., Williams, G.B., Pengas, G., Nestor, P.J., 2010. Absolute diffusivities define the landscape of white matter degeneration in Alzheimer's disease. Brain 133, 529–539. doi:10.1093/brain/awp257.

Adluru, N., Destiche, D.J., Lu, S.Y.F., Doran, S.T., Birdsill, A.C., Melah, K.E., Okonkwo, O.C., Alexander, A.L., Dowling, N.M., Johnson, S.C., Sager, M.A., Bendlin, B.B., 2014. White matter microstructure in late middle-age: effects of apolipoprotein E4 and parental family history of Alzheimer's disease. NeuroImage Clin. 4, 730–742. doi:10.1016/j.nicl.2014.04.008.

Alsop, D.C., Casement, M., de Bazelaire, C., Fong, T., Press, D.Z., 2008. Hippocampal hyperperfusion in Alzheimer's disease. NeuroImage 42, 1267–1274. doi:10.1016/j.neuroimage.2008.06.006.

Alsop, D.C., Dai, W., Grossman, M., Detre, J.A., 2010. Arterial spin labeling blood flow MRI: its role in the early characterization of Alzheimer's disease. J. Alzheimer's Dis. doi:10.3233/JAD-2010-091699.

Alsop, D.C., Detre, J.A., Golay, X., Günther, M., Hendrikse, J., Hernandez-Garcia, L., Lu, H., MacIntosh, B.J., Parkes, L.M., Smits, M., van Osch, M.J.P., Wang, D.J.J., Wong, E.C., Zaharchuk, G., 2015. Recommended implementation of arterial spin-labeled perfusion MRI for clinical applications: a consensus of the ISMRM perfusion study group and the European consortium for ASL in dementia. Magn. Reson. Med. 73, 102–116. doi:10.1002/mrm.25197.

Andersson, J.L.R., Graham, M.S., Drobnjak, I., Zhang, H., Filippini, N., Bastiani, M., 2017. Towards a comprehensive framework for movement and distortion correction of diffusion MR images: within volume movement. NeuroImage 152, 450–466. doi:10.1016/j.neuroimage.2017.02.085.

Andersson, J.L.R., Graham, M.S., Zsoldos, E., Sotiropoulos, S.N., 2016. Incorporating outlier detection and replacement into a non-parametric framework for movement and distortion correction of diffusion MR images. NeuroImage 141, 556–572. doi:10.1016/j.neuroimage.2016.06.058.

Ashburner, J., 2007. A fast diffeomorphic image registration algorithm. NeuroImage 38, 95–113. doi:10.1016/j.neuroimage.2007.07.007.

Bangen, K.J., Restom, K., Liu, T.T., Wierenga, C.E., Jak, A.J., Salmon, D.P., Bondi, M.W., 2012. Assessment of Alzheimer's disease risk with functional magnetic resonance imaging: an arterial spin labeling study. J. Alzheimer's Dis. doi:10.3233/JAD-2012-120292.

Bateman, R.J., Xiong, C., Benzinger, T.L.S., Fagan, A.M., Goate, A., Fox, N.C., Marcus, D.S., Cairns, N.J., Xie, X., Blazey, T.M., Holtzman, D.M., Santacruz, A., Buckles, V., Oliver, A., Moulder, K., Aisen, P.S., Ghetti, B., Klunk, W.E., McDade, E., Martins, R.N., Masters, C.L., Mayeux, R., Ringman, J.M., Rossor, M.N., Schofield, P.R., Sperling, R.A., Salloway, S., Morris, J.C., 2012. Clinical and biomarker changes in dominantly inherited Alzheimer's disease. N. Engl. J. Med. 367, 795–804. doi:10.1056/NEJMoa1202753.

Bates, D., Mächler, M., Bolker, B., Walker, S., 2015. Fitting linear mixed-effects models using lme4. J. Stat. Softw. 67, 1–48. doi:10.18637/jss.v067.i01.

Bennett, I.J., Madden, D.J., Vaidya, C.J., Howard, D.V., Howard, J.H., 2010. Age-related differences in multiple measures of white matter integrity: a diffusion tensor imaging study of healthy aging. Hum. Brain Mapp. doi:10.1002/hbm.20872.

Benzinger, T.L.S., Blazey, T., Jack, C.R., Koeppe, R.A., Su, Y., Xiong, C., Raichle, M.E., Snyder, A.Z., Ances, B.M., Bateman, R.J., Cairns, N.J., Fagan, A.M., Goate, A., Marcus, D.S., Aisen, P.S., Christensen, J.J., Ercole, L., Hornbeck, R.C., Farrar, A.M., Aldea, P., Jasielec, M.S., Owen, C.J., Xie, X., Mayeux, R., Brickman, A., McDade, E., Klunk, W., Mathis, C.A., Ringman, J., Thompson, P.M., Ghetti, B., Saykin, A.J., Sperling, R.A., Johnson, K.A., Salloway, S., Correia, S., Schofield, P.R., Masters, C.L., Rowe, C., Villemagne, V.L., Martins, R., Ourselin, S., Rossor, M.N., Fox, N.C., Cash, D.M., Weiner, M.W., Holtzman, D.M., Buckles, V.D., Moulder, K., Morris, J.C., 2013. Regional variability of imaging biomarkers in autosomal dominant Alzheimer's disease. Proc. Natl. Acad. Sci. U.S.A. 110, E4502–E4509. doi:10.1073/pnas.1317918110.

Buxton, R.B., Frank, L.R., Wong, E.C., Siewert, B., Warach, S., Edelman, R.R., 1998. A general kinetic model for quantitative perfusion imaging with arterial spin labeling. Magn. Reson. Med. 40, 383–396. doi:10.1002/mrm.1910400308, https://doi.org/.

Caballero, M.Á.A., Suárez-Calvet, M., Duering, M., Franzmeier, N., Benzinger, T., Fagan, A.M., Bateman, R.J., Jack, C.R., Levin, J., Dichgans, M., Jucker, M., Karch, C., Masters, C.L., Morris, J.C., Weiner, M., Rossor, M., Fox, N.C., Lee, J.H., Salloway, S., Danek, A., Goate, A., Yakushev, I., Hassenstab, J., Schofield, P.R., Haass, C., Ewers, M., 2018. White matter diffusion alterations precede symptom onset in autosomal dominant Alzheimer's disease. Brain 141, 3065–3080. doi:10.1093/brain/awy229.

Cash, D.M., Ridgway, G.R., Liang, Y., Ryan, N.S., Kinnunen, K.M., Yeatman, T., Malone, I.B., Benzinger, T.L.S., Jack, C.R., Thompson, P.M., Ghetti, B.F., Saykin, A.J., Masters, C.L., Ringman, J.M., Salloway, S.P., Schofield, P.R., Sperling, R.A., Cairns, N.J., Marcus, D.S., Xiong, C., Bateman, R.J., Morris, J.C., Rossor, M.N., Ourselin, S., Fox, N.C., 2013. The pattern of atrophy in familial Alzheimer disease: volumetric MRI results from the DIAN study. Neurology 81, 1425–1433. doi:10.1212/WNL.0b013e3182a841c6.

Chappell, M.A., Groves, A.R., MacIntosh, B.J., Donahue, M.J., Jezzard, P., Woolrich, M.W., 2011. Partial volume correction of multiple inversion time arterial spin labeling MRI data. Magn. Reson. Med. 65, 1173–1183. doi:10.1002/mrm.22641.

Chappell, M.A., Groves, A.R., Whitcher, B., Woolrich, M.W., 2009. Variational Bayesian Inference for a nonlinear forward model. IEEE Trans. Signal Process. 57, 223–236. doi:10.1109/TSP.2008.2005752.

Clark, A.L., Bangen, K.J., Sorg, S.F., Schiehser, D.M., Evangelista, N.D., McKenna, B., Liu, T.T., Delano-Wood, L., 2017. Dynamic association between perfusion and white matter integrity across time since injury in Veterans with history of TBI. NeuroImage Clin. 14, 308–315. doi:10.1016/j.nicl.2016.12.017.

Day, G.S., Cruchaga, C., Wingo, T., Schindler, S.E., Coble, D., Morris, J.C., 2019. Association of acquired and heritable factors with intergenerational differences in age at symptomatic onset of Alzheimer disease between offspring and parents with dementia. JAMA Netw. Open 2, e1913491. doi:10.1001/jamanetworkopen.2019.13491.

Dolui, S., Vidorreta, M., Wang, Z., Nasrallah, I.M., Alavi, A., Wolk, D.A., Detre, J.A., 2017. Comparison of PASL, PCASL, and background-suppressed 3D PCASL in mild cognitive impairment. Hum. Brain Mapp. 38, 5260–5273. doi:10.1002/hbm.23732.

Fazlollahi, A., Calamante, F., Liang, X., Bourgeat, P., Raniga, P., Dore, V., Fripp, J., Ames, D., Masters, C.L., Rowe, C.C., Connelly, A., Villemagne, V.L., Salvado, O., 2020. Increased cerebral blood flow with increased amyloid burden in the preclinical phase of Alzheimer's disease. J. Magn. Reson. Imaging doi:10.1002/jmri.26810.

Firbank, M.J., Minett, T., O'Brien, J.T., 2003. Changes in DWI and MRS associated with white matter hyperintensities in elderly subjects. Neurology 61, 950–954.

Fischl, B., 2012. FreeSurfer. NeuroImage 62, 774–781. doi:10.1016/j.neuroimage.2012.01.021.FreeSurfer.

Fox, J., Monette, G., 1992. Generalized collinearity diagnostics. J. Am. Stat. Assoc. doi:10.1080/01621459.1992.10475190.

Fox, J., Weisberg, S., 2019. CAR – An R Companion to Applied Regression. Sage, Thousand Oaks CA.

Gatz, M., Reynolds, C.A., Fratiglioni, L., Johansson, B., Mortimer, J.A., Berg, S., Fiske, A., Pedersen, N.L., 2006. Role of genes and environments for explaining Alzheimer disease. Arch. Gen. Psychiatry doi:10.1001/archpsyc.63.2.168.

Guillaume, B., Hua, X., Thompson, P.M., Waldorp, L., 2013. Fast and accurate modelling of longitudinal neuroimaging data : an application to ADNI data 2013.

Guillaume, B., Nichols, T.E., Adni, the, 2015. Non-parametric inference for longitudinal and repeated-measures neuroimaging data with the wild bootstrap. Organ. Hum. Brain Mapp. 2.

Habib, M., Mak, E., Gabel, S., Su, L., Williams, G., Waldman, A., Wells, K., Ritchie, K., Ritchie, C., O'Brien, J.T., 2017. Functional neuroimaging findings in healthy middle-aged adults at risk of Alzheimer's disease. Ageing Res. Rev. doi:10.1016/j.arr.2017.03.004.

Honea, R.A., Swerdlow, R.H., Vidoni, E.D., Goodwin, J., Burns, J.M., 2010. Reduced gray matter volume in normal adults with a maternal family history of Alzheimer disease. Neurology 74, 113–120. doi:10.1212/WNL.0b013e3181c918cb.

Jezzard, P., Chappell, M.A., Okell, T.W., 2018. Arterial spin labeling for the measurement of cerebral perfusion and angiography. J. Cereb. Blood Flow Metab. 38, 603–626. doi:10.1177/0271678X17743240.

Kantarci, K., Murray, M.E., Schwarz, C.G., Reid, R.I., Przybelski, S.A., Lesnick, T., Zuk, S.M., Raman, M.R., Senjem, M.L., Gunter, J.L., Boeve, B.F., Knopman, D.S., Parisi, J.E., Petersen, R.C., Jack, C.R., Dickson, D.W., 2017. White-matter integrity on DTI and the pathologic staging of Alzheimer's disease. Neurobiol. Aging 56, 172–179. doi:10.1016/j.neurobiolaging.2017.04.024.

Kantarci, K., Petersen, R.C., Boeve, B.F., Knopman, D.S., Weigand, S.D., O'Brien, P.C., Shiung, M.M., Smith, G.E., Ivnik, R.J., Tangalos, E.G., Jack, C.R., 2005. DWI predicts future progression to Alzheimer disease in amnestic mild cognitive impairment. Neurology 64, 902–904. doi:10.1212/01.WNL.0000153076.46126.E9.

Kodiweera, C., Alexander, A.L., Harezlak, J., McAllister, T.W., Wu, Y.-C., 2016. Age effects and sex differences in human brain white matter of young to middle-aged adults: a DTI, NODDI, and q-space study. NeuroImage 128, 180–192. doi:10.1016/j.neuroimage.2015.12.033.

Lee, S., Viqar, F., Zimmerman, M.E., Narkhede, A., Tosto, G., Benzinger, T.L.S., Marcus, D.S., Fagan, A.M., Goate, A., Fox, N.C., Cairns, N.J., Holtzman, D.M., Buckles, V., Ghetti, B., McDade, E., Martins, R.N., Saykin, A.J., Masters, C.L., Ringman, J.M., Ryan, N.S., Förster, S., Laske, C., Schofield, P.R., Sperling, R.A., Salloway, S., Correia, S., Jack, C., Weiner, M., Bateman, R.J., Morris, J.C., Mayeux, R., Brickman, A.M., 2016. White matter hyperintensities are a core feature of Alzheimer's disease: evidence from the dominantly inherited Alzheimer network. Ann. Neurol. 79, 929–939. doi:10.1002/ana.24647.

Leemans, A., Jones, D.K., 2009. The B-matrix must be rotated when correcting for subject motion in DTI data. Magn. Reson. Med. 61, 1336–1349. doi:10.1002/mrm.21890.

Mak, E., Gabel, S., Mirette, H., Su, L., Williams, G.B., Waldman, A., Wells, K., Ritchie, K., Ritchie, C., O'Brien, J., 2017. Structural neuroimaging in preclinical dementia: from microstructural deficits and grey matter atrophy to macroscale connectomic changes. Ageing Res. Rev. 35, 250–264. doi:10.1016/j.arr.2016.10.001.

McEwen, B.S., 1997. Possible mechanisms for atrophy of the human hippocampus. Mol. Psychiatry 2, 255–262. doi:10.1038/sj.mp.4000254.

Miller, K.L., Alfaro-Almagro, F., Bangerter, N.K., Thomas, D.L., Yacoub, E., Xu, J., Bartsch, A.J., Jbabdi, S., Sotiropoulos, S.N., Andersson, J.L.R., Griffanti, L., Douaud, G., Okell, T.W., Weale, P., Dragonu, I., Garratt, S., Hudson, S., Collins, R., Jenkinson, M., Matthews, P.M., Smith, S.M., 2016. Multimodal population brain imaging in the UK Biobank prospective epidemiological study. Nat. Neurosci. 19, 1523–1536. doi:10.1038/nn.4393.

Montagne, A., Nation, D.A., Sagare, A.P., Barisano, G., Sweeney, M.D., Chakhoyan, A., Pachicano, M., Joe, E., Nelson, A.R., D'Orazio, L.M., Buennagel, D.P., Harrington, M.G., Benzinger, T.L.S., Fagan, A.M., Ringman, J.M., Schneider, L.S., Morris, J.C., Reiman, E.M., Caselli, R.J., Chui, H.C., TCW, J., Chen, Y., Pa, J., Conti, P.S., Law, M., Toga, A.W., Zlokovic, B.V., 2020. APOE4 leads to blood–brain barrier dysfunction predicting cognitive decline. Nature 1–6. doi:10.1038/s41586-020-2247-3.

Müller, M.J., Greverus, D., Dellani, P.R., Weibrich, C., Wille, P.R., Scheurich, A., Stoeter, P., Fellgiebel, A., 2005. Functional implications of hippocampal volume and diffusivity in mild cognitive impairment. NeuroImage 28, 1033–1042. doi:10.1016/j.neuroimage.2005.06.029.

Østergaard, L., Aamand, R., Gutiérrez-Jiménez, E., Ho, Y.C.L., Blicher, J.U., Madsen, S.M., Nagenthiraja, K., Dalby, R.B., Drasbek, K.R., Møller, A., Brændgaard, H., Mouridsen, K., Jespersen, S.N., Jensen, M.S., West, M.J., 2013. The capillary dysfunction hypothesis of Alzheimer's disease. Neurobiol. Aging 34, 1018–1031. doi:10.1016/j.neurobiolaging.2012.09.011.

Pedersen, N.L., Gatz, M., Berg, S., Johansson, B., 2004. How heritable is Alzheimer's disease late in life? Findings from Swedish twins. Ann. Neurol. doi:10.1002/ana.10999.

Reuter, M., Rosas, H.D., Fischl, B., 2012. Longitudinal FreeSurfer for reliable imaging biomarkers. In: Proceedings of the MICCAI Novel Neuroimaging Biomarkers Alzheimer's Disease and Related Disorders Workshop and Challenge, p. 12.

Reuter, M., Rosas, H.D., Fischl, B., 2010. Highly accurate inverse consistent registration: a robust approach. NeuroImage 53, 1181–1196. doi:10.1016/j.neuroimage.2010.07.020.

Ringman, J.M., Medina, L.D., Braskie, M., Rodriguez-Agudelo, Y., Geschwind, D.H., MacIas-Islas, M.A., Cummings, J.L., Bookheimer, S., 2011. Effects of risk genes on BOLD activation in presymptomatic carriers of familial alzheimer's disease mutations during a novelty encoding task. Cereb. Cortex 21, 877–883. doi:10.1093/cercor/bhq158.

Ringman, J.M., O'Neill, J., Geschwind, D., Medina, L., Apostolova, L.G., Rodriguez, Y., Schaffer, B., Varpetian, A., Tseng, B., Ortiz, F., Fitten, J., Cummings, J.L., Bartzokis, G., 2007. Diffusion tensor imaging in preclinical and presymptomatic carriers of familial Alzheimer's disease mutations. Brain 130, 1767–1776. doi:10.1093/brain/awm102.

Ritchie, C.W., Ritchie, K., 2012. The PREVENT study: a prospective cohort study to identify mid-life biomarkers of late-onset Alzheimer's disease. BMJ Open 2, 1–6. doi:10.1136/bmjopen-2012-001893.

Ritchie, C.W., Wells, K., Ritchie, K., 2013. The PREVENT research programme – A novel research programme to identify and manage midlife risk for dementia: the conceptual framework. Int. Rev. Psychiatry 25, 748–754. doi:10.3109/09540261.2013.869195.

Ritchie, K., Carrière, I., Berr, C., Amieva, H., Dartigues, J.-F., Ancelin, M.-L., Ritchie, C.W., 2016. The clinical picture of Alzheimer's disease in the decade before diagnosis: clinical and biomarker trajectories. J. Clin. Psychiatry 77, e305–e311. doi:10.4088/JCP.15m09989.

Ritchie, K., Carrière, I., Su, L., O'Brien, J.T., Lovestone, S., Wells, K., Ritchie, C.W., 2017. The midlife cognitive profiles of adults at high risk of late-onset Alzheimer's disease: the PREVENT study. Alzheimer's Dement. 13, 1089–1097. https://doi.org/10.1016/j.jalz.2017.02.008

Salami, A., Eriksson, J., Nilsson, L.G., Nyberg, L., 2012. Age-related white matter microstructural differences partly mediate age-related decline in processing speed but not cognition. Biochim. Biophys. Acta – Mol. Basis Dis. 1822, 408–415. doi:10.1016/j.bbadis.2011.09.001.

Scarabino, D., Gambina, G., Broggio, E., Pelliccia, F., Corbo, R.M., 2016. Influence of family history of dementia in the development and progression of late-onset Alzheimer's disease. Am. J. Med. Genet. Part B Neuropsychiatr. Genet. 171, 250–256. doi:10.1002/ajmg.b.32399.

Shao, X., Ma, S.J., Casey, M., D'Orazio, L., Ringman, J.M., Wang, D.J.J., 2019. Mapping water exchange across the blood–brain barrier using 3D diffusion-prepared arterial spin labeled perfusion MRI. Magn. Reson. Med. doi:10.1002/mrm.27632.

Smart, S.D., Firbank, M.J., O'Brien, J.T., 2011. Validation of automated white matter hyperintensity segmentation. J. Aging Res. 2011, 391783. doi:10.4061/2011/391783.

Smith, S.M., Nichols, T.E., 2009. Threshold-free cluster enhancement: addressing problems of smoothing, threshold dependence and localisation in cluster inference. NeuroImage 44, 83–98. doi:10.1016/j.neuroimage.2008.03.061.

Stefaniak, J.D., Su, L., Mak, E., Sheikh-bahaei, N., Wells, K., Ritchie, K., Waldman, A., Ritchie, C.W., Brien, J.T.O., 2018. Cerebral small vessel disease in middle age and genetic predisposition to late-onset Alzheimer's disease 14, 253–258. https://doi.org/10.1016/j.jalz.2017.08.017

Villeneuve, S., Vogel, J.W., Gonneaud, J., Pichet Binette, A., Rosa-Neto, P., Gauthier, S., Bateman, R.J., Fagan, A.M., Morris, J.C., Benzinger, T.L.S., Johnson, S.C., Breitner, J.C.S., Poirier, J., Barkun, A., Evans, A., Salaciak, A., Tam, A., Labonté, A., Faubert, A.M., Mathieu, A., Courcot, B., Hyman, B.T., Madjar, C., Carrier, C.E., Dansereau, C., Kazazian, C., Tardif, C., Lepage, C., Cuello, C., Debacker, C., Jack, C.R., Picard, C., Maillet, D., Fontaine, D., Knopman, D.S., Michaud, D., Couture, D., Dea, D., Teigner, E., Anthal, E., Yu, E., Vachon-Presseau, E., Saint-Fort, E.F., Ferdinand, F., Benbouhoud, F., Pogossova, G., Maultaup, G., Mayrand, G., Duclair, G., Ayranci, G., Gagné, G., Newbold-Fox, H., Leppert, I., Vallée, I., Near, J., Brandt, J., Maltais, J.R., Leoutsakos, J.M., Tremblay-Mercier, J., Pruessner, J., Frenette, J., Frappier, J., Kat, J., Miron, J., Wan, K., Cheewakriengkrai, L., Mahar, L., Carmo, L., Münter, L.M., Collins, L., Théroux, L., Dadar, M., Chakravarty, M., Dufour, M., Lafaille-Magnan, M.E., Dauar-Tedeschi, M., Sager, M.A., Eisenberg, M., Appleby, M., Savard, M., Tuwaig, M., Petkova, M., Rajah, N., Aisen, P., Toussaint, P.J., Kostopoulos, P., Bellec, P., Etienne, P., Tariot, P.N., Orban, P., Rioux, P., Meyer, P.F., El-Khoury, R., Sperling, R.A., Desautels, R., Gordon, R., Giles, R., Hoge, R., Thomas, R.G., Das, S., Verfaillie, S.C.J., Farzin, S., Wang, S., Tabrizi, S., Tullo, S., Mathotaarachchi, S., Craft, S., Dubuc, S., Lee, T., Pascoal, T.A., Montine, T.J., Beaudry, T., Gervais, V., Nair, V., Bohbot, V., Pagé, V., Venugopalan, V., Fonov, V., Ituria-Medina, Y., Khachaturian, Z.S., 2018. Proximity to parental symptom onset and amyloid-β burden in sporadic Alzheimer disease. JAMA Neurol. 75, 608–619. doi:10.1001/jamaneurol.2017.5135.

Viqar, F., S., L., M.E., Z., A., N., G., T., T.L.S., B., D.S., M., R.J., B., J.C., M., R., M., 2015. White matter hyperintensities are a core feature of Alzheimer's disease: Evidence from the dominantly inherited Alzheimer's network. Alzheimer's Dement. 11, P172–P173. doi:10.1002/ana.24647.

Vogel, J.W., Vachon-Presseau, E., Pichet Binette, A., Tam, A., Orban, P., La Joie, R., Savard, M., Picard, C., Poirier, J., Bellec, P., Breitner, J.C.S., Villeneuve, S., 2018. Brain properties predict proximity to symptom onset in sporadic Alzheimer's disease. Brain 141, 1871–1883. doi:10.1093/brain/awy093.

Weston, P.S.J., Simpson, I.J.A., Ryan, N.S., Ourselin, S., Fox, N.C., 2015. Diffusion imaging changes in grey matter in Alzheimer's disease: a potential marker of early neurodegeneration. Alzheimers. Res. Ther. 7, 47. doi:10.1186/s13195-015-0132-3.

Wierenga, C.E., Clark, L.R., Dev, S.I., Shin, D.D., Jurick, S.M., Rissman, R.A., Liu, T.T., Bondi, M.W., 2013. Interaction of age and APOE genotype on cerebral blood flow at rest. J. Alzheimer's Dis. 34, 921–935. doi:10.3233/JAD-121897.

Wierenga, C.E., Hays, C.C., Zlatar, Z.Z., 2014. Cerebral blood flow measured by arterial spin labeling MRI as a preclinical marker of alzheimer's disease. J. Alzheimer's Dis. doi:10.3233/JAD-141467.